The elimination of coffee-ring formation by humidity cycling - a numerical study

Adam D. Eales and Alexander F. Routh*

Department of Chemical Engineering, University of Cambridge, Cambridge, CB2 3RA, United Kingdom

E-mail: afr10@cam.ac.uk

Abstract

Periodically switching between evaporation and condensation, or 'humidity cycling', has potential for controlling the film shape that results from volatile droplets containing a non-volatile material. It does not require adaptation of material properties nor the introduction of an external field in order to achieve a change in film shape. It was shown experimentally by Doi and co-workers [Kajiya *et al.*, *Langmuir*, 2010; 26, 10429-10432],[1] that ring-shaped deposits can be removed through careful selection of the atmospheric conditions. In this paper we present a model, based on lubrication theory, which can predict the final film shape resulting from the humidity cycling process. We confirm that the refluidization of gelled regions during condensation and the subsequent inward flow[1] is the mechanism responsible for the improved profiles. Further, we find that an increase in the time spent condensing to that spent evaporating results in flatter films and that an optimal humidity cycling frequency exists.

Introduction

The coffee-ring mechanism was first described by Deegan and co-workers in 1997.[2] If the periphery of a volatile droplet containing solids is pinned, so that it cannot advance nor

recede, a region of enhanced deposition occurs at the edge. This is due to an outward capillary flow, which convects solids to the droplet edge.

For various applications the coffee-ring shape is undesirable. These include but are not limited to DNA microarrays,[3–6] herbicides on leaves[7,8] and inkjet printing applications,[9] such as polymer-organic light emitting diode display devices (P-OLEDs).[10,11] For example, the lifespan of P-OLED displays is related to the current and so the film thickness. An undulating profile results in non-spatially uniform current and hence a shorter lifetime.[12]

Broadly there are two overarching themes used in the prevention of coffee-ring formation. Either the pinning phenomenon is prevented or the outward capillary flow is counteracted, suppressed or dominated by an alternative flow. There are several established methods for mitigation of the ring stain. These are mostly intrusive, since they involve addition of another material or external field, or a change in the properties/size/shape of the liquid and/or the suspended solid.

First, we discuss methods that work by counteracting the dominance of the outward capillary flow.

If a surface tension differential exists, then for positive curvature a flow from regions of low to high surface tension will result. This is termed Marangoni flow. Its origin can either be due to the presence of a solute, for example surfactant,[8,13,14] that reduces the surface tension, or thermally induced, exploiting the temperature dependence of surface tension.[15–17] In these cases, less of the solid material is deposited at the edge.

Addition of an acid or base to change the pH, alters the Derjaguin, Landau, Verwey, Overbeek (DLVO) interactions between the dispersed entities[18] and also between the dispersed phase and substrate.[19] Either aggregation followed by sedimentation or a strong attraction to the substrate can result in a uniform deposit.

By using an ellipsoidal suspended solid, rather than spheres, Yunker *et al.*[20] and Vermant[21] demonstrated that the ring formation can be removed. The droplet surface is deformed by the presence of anisotropic particles, resulting in strong, long-range inter-particle

capillary interactions that cause loosely-packed structures to form. This behaviour dominates over the outward transport.

In contrast, electrowetting techniques work by preventing the pinning phenomenon. Alternating current electrowetting causes the edges of the droplet to periodically advance and recede, to wet and dewet the substrate. This prevents contact line pinning and therefore ring formation does not occur.[22–24] If instead direct current electrowetting is applied, the droplet just depins and recedes.[25,26] It was demonstrated by Wray *et al.*[27] that, through careful field selection, the coffee-ring effect can be avoided.

Whilst significant advances have been made, there are still applications for which the above methods cannot be used, either due to practicality or invasion of the system. For this reason, there are new methods of ring suppression being developed. These include the use of multicomponent liquids,[9,28–36,42] altering the geometry of the substrate,[11,37–39] acoustic suppression[40] and humidity cycling.[1,41] The latter is the focus of the present work.

It was demonstrated experimentally by Doi and co-workers[1,41] that controlling the humidity and cycling between evaporation and condensation can prevent ring formation. It was argued that the condensation causes refluidization of packed/gelled regions and removal of the outward capillary flow. The optimal cycling period and relative times of exposure have yet to be determined. We are not aware of any previous attempts to model the drying dynamics and resulting final film shapes for this technique.

In this paper, we build on our previously reported thin-film lubrication model for the drying dynamics of droplets containing suspended solids.[10,11,42,43] This has similarity to other models that use lubrication theory, such as.[27,44–48]

Mathematical model

Assumptions & simplifications

Consider a droplet consisting of a polymer, with initial volume fraction ϕ_0, and a unary liquid with viscosity μ_0 and surface tension γ_0. Depending on the properties of the surrounding

atmosphere, the liquid will either evaporate or there will be condensation of vapour into the droplet. The local evaporation rate E and condensation rate C are defined on a volumetric flux per unit area basis, (i.e. $m^3\ m^{-2}\ s^{-1}$ or just $m\ s^{-1}$.)

It is assumed that the three-phase contact line, at the edge of the droplet, is unconditionally pinned, throughout the process. The contact line does not recede during periods of evaporation, due to a strong anchoring to the substrate by, for example, adsorption of polymer. Furthermore, to simplify the solution required, it is assumed the contact line does not advance during periods of condensation. In practice this could be realised by placing an obstruction, such as a vertical wall or a superhydrophobic material, at the initial location of the droplet edge.

The coordinate system is cylindrical, with horizontal position r, vertical position z and azimuth θ. This is illustrated in the sketch of the droplet in Figure 1. The height of the liquid/atmosphere interface is h and this is a function of horizontal position and time, t. The vertical length scale H is taken to be the initial centreline height of the droplet. The horizontal length scale R is taken to be half the initial base width.

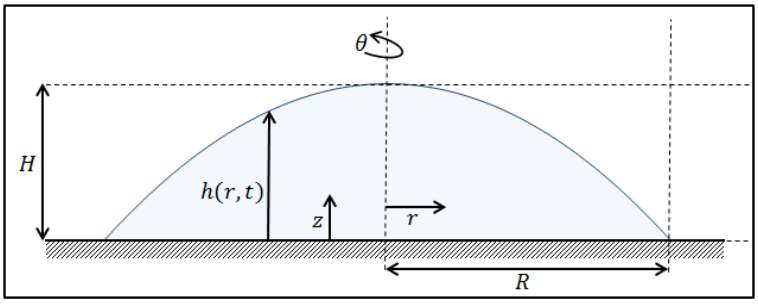

Figure 1: Sketch of a droplet with vertical length scale H and horizontal length scale R, in a cylindrical coordinate frame (r, z, θ).

It is assumed that the droplet is axisymmetric. Hence, the angular velocity and gradients can be ignored ($v_\theta = 0$, $\partial/\partial\theta = 0$).

Typically, the droplets are thin ($H \sim 7\ \mu m$, $R \sim 125\ \mu m$ and hence $H^2/R^2 \ll 1$) and the Reynolds number is small ($Re = \frac{\rho E R}{\mu} \sim 10^{-7}$). The creeping flow scenario and

lubrication approximation are therefore applicable. It can hence be shown that within the droplet, there is negligible pressure gradient in the vertical direction. It is therefore helpful to consider the vertically averaged horizontal velocity $\tilde{v_r} = \frac{1}{h}\int_{z=0}^{z=h} v_r dz$ and ignore depthwise gradients, rather than use the vertical (v_z) and horizontal (v_r) velocities separately.

It can be shown that the Bond number is small ($Bo = \frac{\rho g R^2}{\gamma} \sim 10^{-3}$), such that surface tension dominates distortions of the liquid/atmosphere interface due to gravity. The capillary number is also small ($Ca = \frac{3\mu R^4 E}{\gamma H^4} \sim 10^{-5}$), such that surface tension dominates viscous forces. The polymer Péclet number is typically large ($Pe = \frac{R^2 E}{HD} > 10^1$, where D is the polymer diffusivity). The polymer convection hence dominates diffusion.

It has been shown in previous work[10,46] that the spatial variation of the evaporation rate can affect the shape of the dried polymer film. One can choose from a host of different evaporation models, such as uniform or edge-enhanced, and take into account a plethora of physical effects, such as natural convection. Whilst these may be important for accurate film shape prediction, it is not necessary to account for these complexities if one wishes to understand the underlying trends. As shown in our previous work[10] a coffee-ring results if the contact line is pinned, no matter whether the evaporation profile is uniform or edge-enhanced. Furthermore, the trends in film shape observed with, for example, varying polymer content, are no different. To remove modelling complexity, it is decided to use a spatially uniform evaporation model in this paper, in the same manner as previous works.[10,47] This is justifiable, since we only aim to identify trends with the important groups of the system. In order to make an accurate prediction of film shape, this work could be extended to include a situationally appropriate evaporation model.

There are two different modes of condensation, filmwise and dropwise. The latter occurs if the liquid does not wet the surface it is condensing onto. The result is the formation of droplets at nucleation sites. Apart from a few notable exceptions, for example water, filmwise condensation is more common. Moreover, the condensation in our context is onto a droplet of the same material, rather than onto a solid substrate. It is therefore expected

that condensation will be filmwise. The local condensation rate will depend on the driving force for mass transfer, the humidity differential. One could develop or incorporate a model for the spatial variation of condensation rate. However, for simplicity, it is assumed that the condensation profile is also uniform.

The polymer is assumed to have an initially homogeneous distribution. As evaporation proceeds, the polymer volume fraction will increase. This cannot happen indefinitely, therefore, a maximal value $\phi_{\max}$ is imposed, due to gelation. In regions where $\phi = \phi_{\max}$, the viscosity is very large and the properties exhibited are characteristic of a gel, rather than sol. The height is fixed and does not change with time. When condensation takes place, the polymer volume fraction will decrease, provided that gelled regions can refluidize. The polymer volume fraction cannot become negative but can fall to zero. However, if it does so, we note that the assumption of a pinned contact line would have to be removed. This work does not consider contact line movement, the complexities of which could be considered in future research.

Derivation methodology & governing equations

The final film shape depends, to a great extent, on the strength and direction of the flow within the droplet. Therefore, an expression is needed for the velocity in the liquid. This can be determined from the solution of the Navier-Stokes equations as we have previously reported[10,11,42] by performing a scaling analysis. A 1D flow model can be used because the vertical pressure gradient is small and depthwise composition gradients are negligible, for thin droplets in the lubrication regime. The vertically averaged horizontal velocity, reported in equation 1 can be used in a simplified one-dimensional flow model.

$$\tilde{\bar{v}}_r = \frac{\bar{h}^2}{Ca\ g\left(\phi\right)}\left(\frac{\partial^3 \bar{h}}{\partial \bar{r}^3} + \frac{1}{\bar{r}}\frac{\partial^2 \bar{h}}{\partial \bar{r}^2} - \frac{1}{\bar{r}^2}\frac{\partial \bar{h}}{\partial \bar{r}}\right) \tag{1}$$

where $Ca = \frac{3\mu_0 R^4 E}{\gamma_0 H^4}$ is the capillary number and $g\left(\phi\right)$ is a function that accounts for the increase in viscosity with increased polymer volume fraction, such as the Krieger-Dougherty

equation.

The overbars in equation 1 refer to non-dimensional terms. Height is scaled by H, horizontal position by R and horizontal velocity by RE/H.

By performing a material balance, governing equations can be derived for the height and polymer volume fraction evolution with time t, during both periods of evaporation and condensation. Note that time is scaled by H/E.

For evaporation, the governing equations have been reported previously.[10,11,42]

$$\frac{\partial \bar{h}}{\partial \bar{t}} = -1 - \frac{1}{\bar{r}} \frac{\partial}{\partial \bar{r}} \left[\bar{r} \bar{h} \tilde{\bar{v}}_r \right] \tag{2}$$

$$\frac{\partial \phi}{\partial \bar{t}} = \frac{\phi}{\bar{h}} - \tilde{\bar{v}}_r \frac{\partial \phi}{\partial \bar{r}} + \frac{Pe^{-1}}{\bar{r}\bar{h}} \frac{\partial}{\partial \bar{r}} \left[\bar{r} \bar{h} \frac{\partial \phi}{\partial \bar{r}} \right] \tag{3}$$

For simplicity, the evaporative flux distribution is taken as spatially uniform. The Peclet number, Pe, is the ratio of convective to diffusive polymer transport rate.

During periods of condensation, the governing equations for height and polymer volume fraction are as follows.

$$\frac{\partial \bar{h}}{\partial \bar{t}} = \frac{C}{E} - \frac{1}{\bar{r}} \frac{\partial}{\partial \bar{r}} \left[\bar{r} \bar{h} \tilde{\bar{v}}_r \right] \tag{4}$$

$$\frac{\partial \phi}{\partial \bar{t}} = -\frac{C}{E} \frac{\phi}{\bar{h}} - \tilde{\bar{v}}_r \frac{\partial \phi}{\partial \bar{r}} + \frac{Pe^{-1}}{\bar{r}\bar{h}} \frac{\partial}{\partial \bar{r}} \left[\bar{r} \bar{h} \frac{\partial \phi}{\partial \bar{r}} \right] \tag{5}$$

The group C/E represents the rate of condensation relative to the previous rate of evaporation. The flux distribution for the condensation is taken as spatially uniform.

Boundary & initial conditions

The governing equations for height are fourth order partial differential equations. Four boundary conditions and one initial condition are required for solution.

At the centre of the droplet the boundary conditions are symmetry and zero flux across the centreline.

$$\frac{\partial \bar{h}}{\partial \bar{r}} = 0 \quad \text{at } \bar{r} = 0 \tag{6}$$

$$\bar{r}\bar{h}\tilde{\bar{v}_r} = 0 \quad \text{at } \bar{r} = 0 \tag{7}$$

At the edge of the droplet, the height and velocity are zero.

$$\bar{h} = 0 \quad \text{at } \bar{r} = 1 \tag{8}$$

$$\tilde{\bar{v}_r} = 0 \quad \text{at } \bar{r} = 1 \tag{9}$$

The initial shape of the droplet is taken to be a spherical cap. The droplet relaxes to this shape in order to minimise surface energy.

$$\bar{h}\left(\bar{r}, \bar{t} = 0\right) = 1 - \bar{r}^2 \quad \text{for } 0 \leq \bar{r} \leq 1 \tag{10}$$

Soon after evaporation of the droplet has commenced, a gelled region forms at the edge of the droplet and a front of gelled material then gradually moves inward. It is possible to track the location of this moving liquid/gel interface, $\bar{r_f}$, by using a volume tracking method[43] that we have developed. The governing equation 2 only applies to the liquid region, experiencing an evaporation process. The outer boundary conditions must therefore be altered for the situation where the liquid/gel front is not at the droplet edge.

$$\bar{h} = \bar{h_f} \quad \text{at } \bar{r} = \bar{r_f} \tag{11}$$

$$\bar{v}_r|_{\bar{r}=\bar{r}_\mathrm{f}} = \frac{(1-f_\mathrm{h})\int_{\bar{r}_\mathrm{f}}^{1}\bar{r}\bar{E}\,(\bar{r})\,d\bar{r}}{\bar{r}_\mathrm{f}\bar{h}_\mathrm{f}} \quad \text{at } \bar{r}=\bar{r}_\mathrm{f} \tag{12}$$

where $\bar{h}_f$ is the height at the liquid/gel front location and $\bar{f}_h$ is the fraction by which the evaporation is suppressed in gelled regions.

For the solution of the governing equations for polymer content, an additional boundary and initial condition are needed.

$$\frac{\partial\phi}{\partial\bar{r}} = 0 \quad \text{at } \bar{r}=0 \tag{13}$$

$$\phi\,(\bar{r},\bar{t}=0) = \phi_0 \quad \text{for } 0\leq\bar{r}\leq 1 \tag{14}$$

The switch from evaporation to condensation and vice versa is considered in the fast limit. In this manner, the code switches from solving equations 2 and 3 to solving equations 4 and 5, in the next time-step. If one wished to model a more gradual process, the evaporation/condensation terms in equations 2 and 3 could be adapted and written in terms of the humidity differential and a separate equation could subsequently be used to evolve the vapour concentration in the atmosphere.

Groups that we will consider

Our focus is solely on the humidity cycling process. The influence of material properties is not considered in this work, instead refer to our previous papers.[10,42]

There are two scenarios to consider. The cases where condensation does and does not cause refluidization of gelled regions. For each of these, the influence of three dimensionless groups on the final film shape is to be considered. First, the relative rate of condensation to evaporation, C/E, taken as constant for simplicity. Second, the relative period of time spent condensing to that spent evaporation, $\bar{t}_c/\bar{t}_e$. Third, the frequency of the humidity cycling, f_{hc}, where $f_{hc} = (\bar{t}_e + \bar{t}_c)^{-1}$.

Results

It is not straightforward to measure the extent of coffee-ring formation or how flat a film is. Visual inspection is often no worse than using a more involved mathematical description, such as considering the residuals from a perfect rectangle. With ring-shaped patterns, the profile non-uniformity is most pronounced when the peak height of the peripheral ring is tall and little material is deposited in the centre. We will therefore measure the extent of coffee-ring formation using our measure CR,[10,11,42] defined below

$$CR = \frac{\bar{h}_p}{\bar{h}_c} \tag{15}$$

Where $\bar{h}_p$ is the maximum height of the peripheral ring in the final film profile and $\bar{h}_c$ is the final central height. A large CR represents a large extent of coffee-ring formation.

The influence of refluidization

Doi and co-workers[1] observed an improved film shape by using the humidity cycling process. They argued that this was due to refluidization of the gelled region that forms at the edge of the droplet during the evaporation process.

We investigate this hypothesis numerically. First, we do not allow refluidization of gelled regions. The condensation equations 4 and 5 are therefore solved only in the liquid region up to the gelled front location and the height and polymer volume fraction are fixed in the gelled region. Second, we allow refluidization of gelled regions and extend the domain of the equations 4 and 5 to the edge of the droplet.

In the absence of humidity cycling a pronounced ring is observed. It was found that the final film profile is no different when humidity cycling is employed without refluidization of gelled regions. If however refluidization of gelled regions does occur, the group CR is smaller and so the extent of ring formation is reduced. Figure 2 shows an example of the final film profile with and without refluidization of gelled regions.

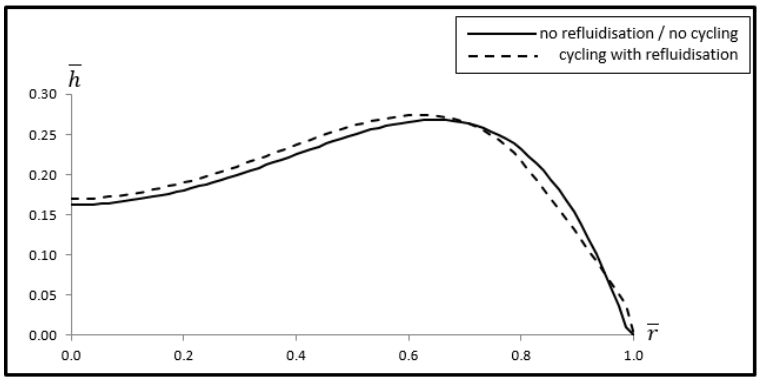

Figure 2: The final film profile with and without refluidization. The results are shown for $Ca = 10^{-3}$, $\phi_0/\phi_{\max} = 0.4$, $f_{\rm h} = 1$, $Pe \to \infty$, $C/E = 0.125$, $\bar{t}_c/\bar{t}_e = 0.0625$ and $f_{hc} = 40$.

Without refluidization, the material transported to the edge of the droplet by the capillary flow, during periods of evaporation, becomes fixed by the gelation process. With refluidization, this material can return to the droplet centre because the surface shape attempts to relax to a spherical cap shape during periods of condensation, to minimise its surface energy. The parameters chosen for the humidity cycling scenario in Figure 2 give only a subtle improvement to the final film shape. Depending on the magnitude of the groups C/E, $\bar{t}_c/\bar{t}_e$ and f_{hc}, differing extents of coffee-ring removal are experienced. This will be discussed in the following sections.

The influence of the relative rate of condensation to evaporation

The relative rate of condensation to evaporation, C/E, has little effect on the final film profile. Figure 3 shows the final film profile for different values of C/E.

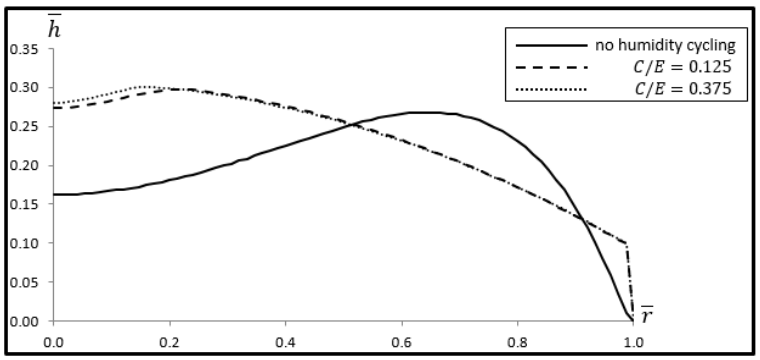

Figure 3: The final film profile as a function of C/E. The results are shown for $Ca = 10^{-3}$, $\phi_0/\phi_{\max} = 0.4$, $f_{\rm h} = 1$, $Pe \to \infty$, $\bar{t}_c/\bar{t}_e = 0.25$ and $f_{hc} = 40$.

Note that the stepped height profile at the droplet edge in Figure 3 is due to the placement of a boundary wall, which prevents the outward movement of the contact line during condensation.

As shown in Figure 3, there is a very marginal decrease in the extent of coffee-ring formation, considering the measure CR, when C/E is increased. This is despite the delayed progression of the liquid/gel front. As shown in Figure 4, a switch to a condensing atmosphere causes the liquid/gel front location to recede back to the droplet edge. This is due to refluidization. The effect is a delayed liquid/gel front propagation, when performing humidity cycling.

With a delayed front progression one would expect an increase in the extent of coffee-ring formation because the capillary flow would act for a longer period of time before the height is fixed by gelation. The reason that the coffee-ring effect is instead reduced is that, following equation 5, an increased C/E causes a further depletion in polymer content near the droplet edge.

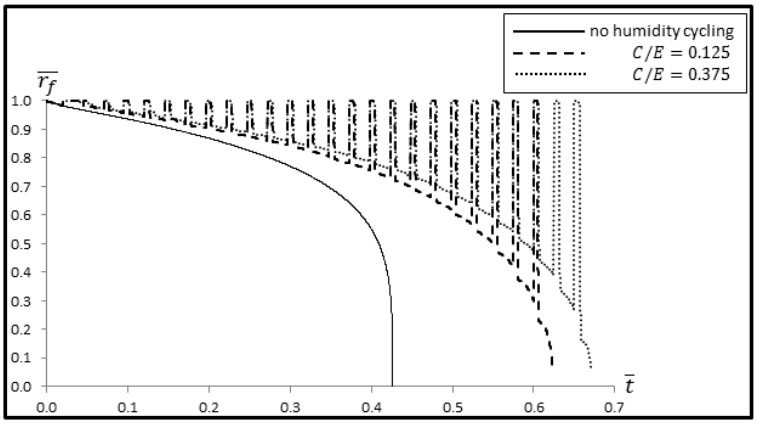

Figure 4: The liquid/gel front position as a function of dimensionless time and C/E. The results are shown for $Ca = 10^{-3}$, $\phi_0/\phi_{\max} = 0.4$, $f_{\rm h} = 1$, $Pe \to \infty$, $\bar{t}_c/\bar{t}_e = 0.25$ and $f_{hc} = 40$.

It will be shown in the following sections that the relative exposure times to condensation and evaporation and the frequency of the humidity cycle are more important than C/E in determination of film shape.

The influence of the relative period of time spent condensing to that spent evaporating

Figure 5 shows the final film profile as a function of the relative period of time spent condensing to that spent evaporating, $\bar{t}_c/\bar{t}_e$.

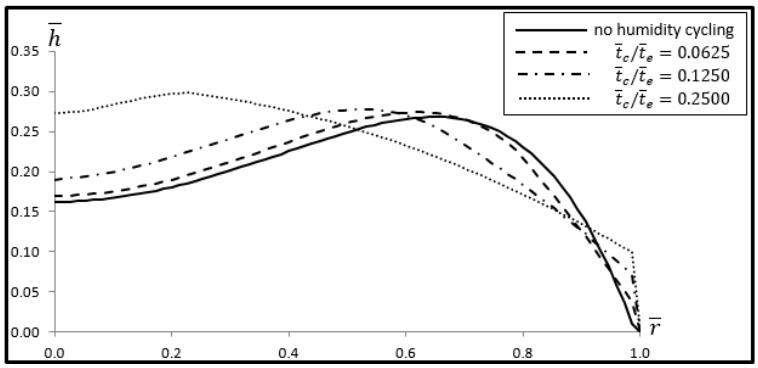

Figure 5: The final film profile as a function of $\bar{t}_c/\bar{t}_e$. The results are shown for $Ca = 10^{-3}$, $\phi_0/\phi_{\max} = 0.4$, $f_{\rm h} = 1$, $Pe \to \infty$, $C/E = 0.125$ and $f_{hc} = 40$.

The humidity cycling procedure decreases the extent of coffee-ring formation. The rel-

ative exposure times of condensation and evaporation controls the extent of film profile improvement. During periods of condensation, refluidization of gelled regions occurs. The ring shape is levelled as the droplet, now absent of gelled regions, attempts to achieve a spherical cap surface shape to minimise its surface energy. The result is an inward flow which drops the height towards the edge and increases the height in the central region. This flow convects the dispersed polymer towards the centre. During periods of evaporation, the outward capillary flow still dominates and convects polymer back towards the edge. When the group $\bar{t}_c/\bar{t}_e$ is larger, the relative time spent with an inward flow scenario is increased. The extent of coffee-ring formation is hence reduced, considering the measure CR.

For $\bar{t}_c/\bar{t}_e = 0.25$, the profile in Figure 5, is almost a perfect spherical cap. Using the measure CR this profile is considered to be good. However, it is far from uniform and for some applications, such as P-OLED displays, this shape would still be undesirable. In these cases a situational dependent coffee-ring measure may prove to be more useful. For example if a more rectangular profile were desired, it may be prudent to decrease $\bar{t}_c/\bar{t}_e$. An optimal value of $\bar{t}_c/\bar{t}_e$ may exist.

As noted previously, we consider the contact line to be perfectly pinned throughout the lifetime of the drying process. The outer boundary of the droplets cannot advance during periods of condensation. This is a good assumption when the outer boundaries are confined in some way, for example by a solid wall, as is the case in the pixel troughs of P-OLED displays. However if this obstacle were removed, a complicated dynamic wetting problem would result. Furthermore, in situations where $f_{hc} = 40$ and $\bar{t}_c/\bar{t}_e > 0.3$, condensation causes the polymer volume fraction to drop to zero in the region near the edge of the droplet. This would cause depinning of the contact line. Upon recommencement of evaporation, repinning of the contact line could occur at a location closer to the centre than the original extremity of the droplet. The complexities of these moving boundary situations await solution.

The influence of the humidity cycling frequency

Figure 6 shows the final film profile as a function of the humidity cycling frequency, $f_{hc} = (\bar{t}_e + \bar{t}_c)^{-1}$.

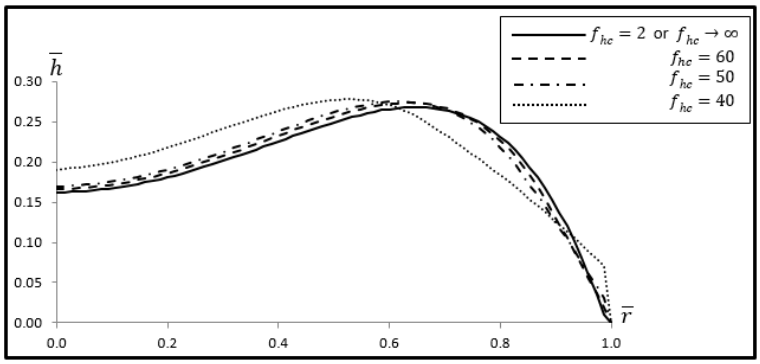

Figure 6: The final film profile as a function of the humidity cycling frequency f_{hc}. The results are shown for $Ca = 10^{-3}$, $\phi_0/\phi_{\max} = 0.4$, $f_{\rm h} = 1$, $Pe \to \infty$, $C/E = 0.125$ and $\bar{t}_c/\bar{t}_e = 0.125$.

The refluidization of gelled regions during condensation and the subsequent inward flow to minimise surface energy on the droplet surface is the mechanism responsible for the improvement in film shape. If the humidity cycling procedure is oscillated too rapidly, as in the limit $f_{hc} \to \infty$, no improvement in film shape is gained. This is because there is not enough time for the spherical cap shape to be restored before evaporation proceeds again, causing further ring formation. If on the other hand the humidity cycling frequency is too small, no improvement in film shape is gained. The condensation does restore the shape but the second period of evaporation acts for a long time and reforms the coffee-ring. This behaviour suggests that there is an optimal humidity cycling frequency. The optimal frequency is likely to be a function of the relative exposure time $\bar{t}_c/\bar{t}_e$, the polymer content $\phi_0/\phi_{\max}$ and the evaporation suppression factor in gelled regions $f_{\rm h}$.

From a practical standpoint, it is important to know how many complete humidity cycles are possible within the total drying time. This is $\bar{t}_f \times f_{hc}$, where $\bar{t}_f$ is the total drying time and depends on both C/E and $\bar{t}_c/\bar{t}_e$. Typically $f_{hc} > 2$ is required for there to be more than one complete humidity cycle. For the $f_{hc} = 40$ plot in Figure 6, there are 24 complete cycles.

In situations where $\bar{t}_c/\bar{t}_e = 0.125$ and $2 < f_{hc} < 35$, condensation causes the polymer volume fraction to drop to zero in the region near the edge of the droplet. The resulting moving boundary problem that develops upon recommencement of evaporation awaits solution.

Conclusion

Controlling the film shape that results from drying of volatile droplets containing a dispersed non-volatile material is important in many fields. In some applications, for example the fabrication of P-OLED displays it is desirable to achieve a flat film.

A number of methods have been developed to try to prevent ring shaped deposits. These include introducing Marangoni flows, addition of acid or base to change the pH and alter the DLVO interactions, using an ellipsoidal suspended solid and employing electrowetting. For various reasons, none of these methods are ideal for P-OLED applications. Instead we have focused on Humidity Cycling, which has potential since it does not require the alteration of material properties or the introduction of an external field.

It was previously shown experimentally by Doi and co-workers[1] that switching between evaporation and condensation could suppress the formation of coffee-rings. They postulated that the reason was refluidization of gelled regions followed by an inward flow. We have confirmed this theory numerically by using a model based on lubrication theory. Moreover, the refluidization is crucial and without this, a coffee-ring would still develop.

For fixed material properties, we have identified 3 groups that control the final film shape that results from the humidity cycling process.

First, the relative rate of condensation to evaporation C/E, which was taken to be temporally invariate for simplicity. This group was shown to have little effect on the final profile.

Second, the exposure time to a condensing atmosphere relative to the time in an evaporative atmosphere, $\bar{t}_c/\bar{t}_e$. Increasing $\bar{t}_c/\bar{t}_e$ causes a reduction in the coffee-ring effect. This is because the inward flow acts for a longer period of time before evaporation recommences.

For some applications, a perfect spherical cap deposit is undesirable. In these situations an optimal value of $\bar{t}_c/\bar{t}_e$ may exist because a certain extent of outward flow may be desirable.

Third, the frequency of the humidity cycling process, $f_{hc} = (\bar{t}_e + \bar{t}_c)^{-1}$. An optimal frequency exists for eliminating the coffee-ring effect. If the humidity oscillation is too rapid, there is not enough time for the surface shape to be restored during periods of condensation. If the humidity oscillation is too slow, any improvement during the condensation period is reversed by the extended evaporation period which follows.

Our solution is only valid when the outer boundaries of the droplet are fixed, for example by the walls of a pixel in a P-OLED display. A focus for future work could be to consider the moving boundary problem at the droplet edge, since for unbounded flat substrates condensation is expected to cause the contact line to advance. This future development could also help to solve the problem we have noted under certain system conditions in which the condensation causes depinning and receding of the contact line.

Acknowledgement

We would like to thank Nick Dartnell and Simon Goddard for useful discussions throughout the duration of our wider project on film formation in drying droplets.

References

(1) **Kajiya T, Kobayashi W, Okuzono T, Doi M.** Controlling profiles of polymer dots by switching between evaporation and condensation. *Langmuir*. 2010; 26: 10429-10432.

(2) **Deegan RD, Bakajin O, Dupont TF, Huber G, Nagel SR, Witten TA.** Capillary flow as the cause of ring stains from dried liquid drops. *Nature*. 1997; 389: 827-829.

(3) **Goldmann T, Gonzalez JS.** DNA-printing: utilization of a standard inkjet printer

for the transfer of nucleic acids to solid supports. *J. Biochem. Bioph. Methods*. 2000; 42: 105-110.

(4) **Angenendt, P.** Progress in protein and antibody microarray technology. *Drug Discovery Today*. 2005; 10: 503-511.

(5) **Heim T, Preuss S, Gerstmayer B, Bosio A, Blossey R.** Deposition from a drop: morphologies of unspecifically bound DNA. *J. Phys.: Condens. Matter*. 2005; 17: S703-S715.

(6) **Deng Y, Zhu XY, Kienlen T, Guo A.** Transport at the air/water interface is the reason for rings in protein microarrays. *J. American Chem. Soc.*. 2006; 128: 2768-2769.

(7) **Faers MA, Pontzen R.** Factors influencing the association between active ingredient and adjuvant in the leaf deposit of adjuvant-containing suspoemulsion formulations. *Pest Management Science*. 2008; 64: 820-833.

(8) **Basi S, Hunsche M, Noga G.** Effects of surfactants and the kinetic energy of monodroplets on the deposit structure of glyphosate at the micro-scale and their relevance to herbicide bio-efficacy on selected weed species. *Weed Research*. 2013; 53: 1-11.

(9) **de Gans BJ, Schubert US.** Inkjet printing of well-defined polymer dots and arrays. *Langmuir*. 2004; 20: 7789-7793

(10) **Eales AD, Dartnell N, Goddard S, Routh AF** Evaporation of pinned droplets containing polymer - an examination of the important groups controlling final shape. *AIChE J*. 2015; 61: 1759-1767.

(11) **Eales AD, Dartnell N, Goddard S, Routh AF** The impact of trough geometry on film shape. A theoretical study of droplets containing polymer, for P-OLED display applications. *J. Colloid Interface Sci.* 2015; 458: 53-61.

(12) **Routh AF.** Drying of thin colloidal films. *Rep. oProg. Phys.* 2013; 76: 046603-1-30.

(13) **Sempels W, De Hier R, Mizuno H, Hofkens J, Vermant J.** Auto-production of biosurfactants reverses the coffee-ring effect in a bacterial system. *Nature Communications*. 2012; 4: 1757-1-8.

(14) **Still T, Yunker PJ, Yodh AG.** Surfactant-induced Marangoni eddies alter the coffee-rings of evaporating colloidal drops. *Langmuir*. 2012; 28: 4984-4988.

(15) **Hu H, Larson RG.** Analysis of the effects of Marangoni stresses on the microflow in an evaporating sessile droplet. *Langmuir*. 2005; 21: 3972-3980.

(16) **Hu H, Larson RG.** Marangoni effect reverses coffee-ring depositions. *J. Phys. Chem. B*. 2006; 110: 7090-7094.

(17) **Ristenpart WD, Kim PG, Domingues C, Wan J, Stone HA.** Influence of substrate conductivity on circulation reveral in evaporating drops. *Phys. Rev. Lett.* 2010; 99: 234502-1-4.

(18) **Dugyala VR, Basavaraj MG.** Control over Coffee-Ring Formation in Evaporating Liquid Drops Containing Ellipsoids. *Langmuir*. 2014; 30: 8680-8686.

(19) **Bhardwaj R, Fang X, Somasundaran P, Attinger D.** Self-Assembly of Colloidal Particles from Evaporating Droplets: Role of DLVO Interactions and Proposition of a Phase Diagram. *Langmuir*. 2010; 26: 7833-7842.

(20) **Yunker PJ, Still T, Lohr MA, Yodh AG.** Suppression of the coffee-ring effect by shape-dependent capillary interactions. *Nature*. 2011; 476: 308-311.

(21) **Vermant J.** Fluid mechanics: When shape matters. *Nature*. 2011; 476: 286-287.

(22) **Eral HB, Mampallil Augustine D, Duits MHG, Mugele F** Suppressing the coffee stain effect: how to control colloidal self-assembly in evaporating drops using electrowetting. *Soft Matter*. 2011; 7: 4954-4958.

(23) **Eral HP, van den Ende D, Mugele F.** Say goodbye to coffee stains. *Physics World*. April 2012: 33-37.

(24) **Mampallil Augustine D, Eral HP, van den Ende D, Mugele F.** Control of evaporating complex fluids through electrowetting. *Soft Matter*. 2012; 8: 10614-10617.

(25) **Yeo LY, Craster RV, Matar OK.** Drop manipulation and surgery using electric fields. *J. Colloid Interface Sci.* 2007; 306: 368-378.

(26) **Orejon D, Sefiane K, Shanahan MER.** Electrostatic suppression of the "coffee stain effect". *J. Colloid Interface Sci.* 2013; 47: 29-38.

(27) **Wray AW, Papageorgiou DT, Craster RV, Sefiane K, Matar OK.** Electrostatic suppression of the coffee-stain effect. *Langmuir*. 2014; 30: 5849-5858.

(28) **Tekin E, de Gans BJ, Schubert US.** Inkjet printing of polymers: from single dots to thin film libraries. *J. Mater. Chem.* 2004; 14: 2627-2632.

(29) **Park J, Moon J.** Control of colloidal particle deposit patterns within picoliter droplets ejected by inkjet printing. *Langmuir*. 2006; 22: 3506-3513.

(30) **Kaneda M, Hyakuta K, Takao Y, Ishizuka H, Fukai J.** Internal flow in polymer solution droplets depsoited on a lyophobic surface during a receding process. *Langmuir*. 2008; 24: 9102-9109.

(31) **Bright CJ, Carter J, Cacheiro M, Lyon P.** US Patent 2010 / 7807070. *Ink jet deposition; comprises electroluminescent material deposited on substrate dissolved in solvent system comprising first high boiling solvent which exhibits low solubility of material to be deposited, and second low boiling solvent which exhibits high solubility of material to be deposited*. Cambridge Display Technology Ltd. Priority Date Feb 27, 2001. Filing Date Oct 9, 2008.

(32) **Wu Y, Eliyahu J, Liu P, Hu NX.** US Patent 2012 / 0232206. *Solvent-based inks comprising silver nanoparticles*. Xerox Corporation. Priority Date Mar 7, 2011. Filing Date Mar 7, 2011.

(33) **Babatunde PO, Hong WJ, Makaso K, Fukai J.** Effect of solute and solvent derived Marangoni flows on the shape of polymer films formed from drying droplets. *AIChE J.* 2013; 59: 699-702.

(34) **Kölpin N, Wegener M, Teuber E, Polster S, Frey L, Roosen A** Conceptional design of nano-particulate ITO inks for inkjet printing of electron devices. *J. Mater. Sci.* 2013; 48: 1623-1631.

(35) **Talbot EL, Berson A, Yang L, Bain CD.** Internal flows and particle transport inside picoliter droplets of binary solvent mixtures. *NIP29: 29th International Conference on Digital Printing Technologies and Digital Fabrication, Seattle, USA, Sep 29 - Oct 3 2013*; 307-312.

(36) **Teichler A, Perelaer J, Schubert US.** Screening of film formation qualities of various solvent systems for π conjugated polymers via combinatorial inkjet printing. *Macromol. Chem. Phys.* 2013; 214: 547-555.

(37) **Okuzono T, Kobayashi M, Doi M.** Final shape of a drying thin film. *Phys. Rev. E.* 2009; 80: 021603.

(38) **Jung Y, Kajiya T, Yamaue T, Doi M.** Film formation kinetics in the drying process of polymer solution enclosed by bank, *Japanese Journal of Applied Physics.* 2009; 48: 031502.

(39) **Kajiya T, Kobayashi W, Okuzono T, Doi M.** Controlling the drying and film formation processes of polymer solution droplets with addition of small amounts of surfactants, *J. Phys. Chem. B.* 2009; 113, 15460-15466.

(40) **Mampallil Augustine D, Reboud J, Wilson R, Wylie D, Klug D, Cooper JM.** Acoustic suppression of the coffee-ring effect. *Soft Matter*. 2015; DOI: 10.1039/C5SM01196E.

(41) **Kajiya T, Doi M.** Dynamics of drying process of polymer solution droplets: analysis of polymer transport and control of film profiles. *Journal of the Society of Rheology, Japan*. 2011; 39: 17-28.

(42) **Eales AD, Dartnell N, Goddard S, Routh AF** Thin, binary liquid droplets, containing polymer: an investigation of the parameters controlling film shape. *In review for J. Fluid Mech.* JFM-15-S-0660.

(43) **Eales AD, Routh AF** A method for continuously tracking the liquid/gel interface, in a drying droplet containing solids. *Unpublished, available upon request.*

(44) **Routh AF, Russel WB.** Horizontal drying fronts during solvent evaporation from latex films. *AIChE J.* 1998; 44: 2088-2098

(45) **Salamanca JM, Ciampi E, Faux DA, Glover PM, McDonald PJ, Routh AF, Peters ACIA, Satguru R, Keddie JL.** Lateral drying in thick films of waterborne colloidal particles. *Langmuir*. 2001; 17: 3202-3207.

(46) **Fischer BJ.** Particle convection in an evaporating colloidal droplet. *Langmuir*. 2002; 18: 60-67.

(47) **Ozawa K, Nishitani E, Doi M.**, Modeling of the Drying Process of Liquid Droplet to Form Thin Film. *Jpn. J. Appl. Phys*. 2005; 44: 4229-4234.

(48) **Tarasevich YY, Vodolazskaya IV, Bondarenko OP.** Modeling of spatial-temporal distribution of the components in the drying sessile droplet of biological fluid. *Colloids Surf., A* . 2013; 432: 99-103.

Table of Contents Graphic